

## Long-wave anisotropic behavior of highly heterogeneous fractured Biot media

Robiel Martínez Corredor , Facultad de Ingeniería, Universidad Nacional de La Plata and Juan E. Santos \*, Instituto del Gas y del Petróleo, Facultad Ingeniería, Universidad de Buenos Aires, Department of Mathematics, Purdue University and Universidad Nacional de La Plata.

### SUMMARY

A Biot medium having a dense set of aligned fractures behaves as an effective transversely isotropic and viscoelastic (TIV) medium at the macroscale for wavelengths much larger than the average distance between fractures. In this work fractures within a Biot medium are represented using boundary conditions imposing stress continuity, pressure discontinuities proportional to average fluid velocities and displacement discontinuities proportional to stress components and average fluid pressures along fractures. These boundary conditions take into account mesoscale effects like wave-induced fluid flow and fluid-pressure changes across fractures. A set of time-harmonic Finite Element experiments is used to determine the stiffness coefficients of an equivalent TIV medium to a highly heterogeneous fractured Biot medium with aligned fractures.

### INTRODUCTION

Hydrocarbon reservoir rocks have in many cases plane compliant discontinuities, like fractures and faults, that in general control the hydrocarbon flow and production in the reservoir Gurevich, B. (2003), Gurevich, B. et al. (2009). Also, in many cases reservoirs rocks contain dense sets of fractures aligned in preferred directions. A fracture in a fluid-saturated poroelastic - Biot - medium is a very thin compliant and highly permeable layer, with the layer thickness on the order of millimeters. In this paper, fractures are modeled using the boundary conditions (B.C.) in Nakawa, S. and Schoenberg, M. A. (2007). These B.C. impose continuity of the stress of the bulk material, pressure discontinuities proportional to average fluid velocities and displacement discontinuities proportional to stress components and average fluid pressures along fractures. Wave-induced fluid flow Santos, J. E. et al. (2011); Santos et al. (2014), by which the fast waves are converted to slow (diffusive) Biot waves when traveling across fractures (mesoscopic-loss) is well represented by these conditions.

A Biot medium with a dense set of horizontal fractures behaves as a transversely isotropic and viscoelastic (TIV) medium for average fracture distances much smaller than the predominant wavelengths of the traveling waves.

The relaxed and unrelaxed stiffnesses of the equivalent poro-viscoelastic medium to a finely layered horizontally homogeneous material were determined in Gelinsky, S. and Shapiro, S. A. (1997). Later, the five complex and frequency-dependent stiffnesses of the equivalent TIV medium were derived in Krzikalla, F. and Müller, T. (2011).

This work uses the set of five harmonic Finite Element (HFE) compressibility and shear experiments described in Santos, J.

E. et al. (2011); Santos et al. (2014) to determine the stiffness coefficients and the corresponding energy velocities and dissipation factors of a long-wave equivalent TIV medium to a horizontally fractured Biot medium. First, the results of the HFE experiments are validated by comparison with those obtained using the HFE experiments when fractures are represented as thin layers as in Santos et al. (2014). Second, the procedure is applied to analyze the response of a fractured Biot medium for variable fracture aperture. Finally, the HFE experiments are applied to analyze the sensitivity of energy velocities in a fractured Biot medium with different volume fractions of fractally varying heterogeneities.

### A FRACTURED BIOT MEDIUM AND THE EQUIVALENT TIV MEDIUM

We consider a fractured isotropic Biot medium  $\Omega = (0, L_1) \times (0, L_3)$  with boundary  $\Gamma$  in the  $(x_1, x_3)$ -plane, with  $x_1$  and  $x_3$  being the horizontal and vertical coordinates, respectively. Let  $\mathbf{u}_s$  and  $\mathbf{u}_f$ , denote the averaged displacement vectors of the solid and fluid phases, respectively. Let  $\mathbf{u}_f = \phi(\mathbf{u}_f - \mathbf{u}_s)$  be the relative fluid displacement, where  $\phi$  denotes the porosity and set  $\mathbf{u} = (\mathbf{u}_s, \mathbf{u}_f)$ . Let  $\mathcal{E}(\mathbf{u}_s)$ ,  $\boldsymbol{\tau}(\mathbf{u})$  and  $p_f(\mathbf{u})$  denote the strain tensor of the solid, the stress tensor of the bulk material and the fluid pressure, respectively. The stress-strain relations are (Biot, M.A., 1962):

$$\boldsymbol{\tau}_{st}(\mathbf{u}) = 2G \boldsymbol{\varepsilon}_{st}(\mathbf{u}_s) + \delta_{st}(\lambda_U \nabla \cdot \mathbf{u}_s + \alpha M \nabla \cdot \mathbf{u}_f), \quad (1)$$

$$p_f(\mathbf{u}) = -\alpha M \nabla \cdot \mathbf{u}_s - M^{(\theta)} \nabla \cdot \mathbf{u}_f. \quad (2)$$

in (1)  $G$  is the shear modulus of the dry matrix and  $\delta_{st}$  is the Kronecker delta. The other coefficients in (1)-(2) can be obtained in terms of  $K_s, K_m$  and  $K_f$ , the bulk moduli of the solid grains, dry matrix and saturant fluid, respectively, (Carcione, 2007). Biot's equations in the diffusive range and in the absence of external forces are (Biot, M.A., 1962):

$$\nabla \cdot \boldsymbol{\tau}(\mathbf{u}) = 0, \quad (3)$$

$$i\omega \mathbf{u}_f + \frac{\mu}{\kappa} \nabla p_f(\mathbf{u}) = 0, \quad (4)$$

where  $i = \sqrt{-1}$ ,  $\omega$  is the angular frequency,  $\mu$  is the fluid viscosity and  $\kappa$  is the frame permeability.

Assume that  $\Omega$  has a set of  $J^{(f)}$  horizontal fractures  $\Gamma^{(f,l)}$ ,  $l = 1, \dots, J^{(f)}$ , each one of length  $L_1$  and aperture  $h$ , so that  $\Omega = \cup_{l=1}^{J^{(f)}+1} R^{(l)}$ . Consider a fracture  $\Gamma^{(f,l)}$  and the two rectangles  $R^{(l)}$  and  $R^{(l+1)}$  having as a common side  $\Gamma^{(f,l)}$ . Let  $\mathbf{v}_{l,l+1}$  and  $\boldsymbol{\chi}_{l,l+1}$  be the unit outer normal and a unit tangent (oriented counterclockwise) on  $\Gamma^{(f,l)}$  from  $R^{(l)}$  to  $R^{(l+1)}$ . Let  $[\mathbf{u}_s], [\mathbf{u}_f]$  denote the jumps of the solid and fluid displacement vectors at  $\Gamma^{(f,l)}$ , i.e.  $[\mathbf{u}_s] = \left( \mathbf{u}_s^{(l+1)} - \mathbf{u}_s^{(l)} \right) |_{\Gamma^{(f,l)}}$ , where  $\mathbf{u}_s^{(l)}$  denotes

## Anisotropy induced by fractures in porous media

the displacement values in  $R^{(l)}$ . The following boundary conditions at  $\Gamma^{(f,l)}$  are derived in Nakawa, S. and Schoenberg, M. A. (2007):

$$[\mathbf{u}_s \cdot \mathbf{v}_{l,l+1}] = \eta_N \left( (1 - \alpha \tilde{B}(1 - \Pi)) \tau(\mathbf{u}) \mathbf{v}_{l,l+1} \cdot \mathbf{v}_{l,l+1} - \alpha \frac{1}{2} \left( (-p_f^{(l+1)}) + (-p_f^{(l)}) \right) \Pi \right), \quad (5)$$

$$[\mathbf{u}_s \cdot \boldsymbol{\chi}_{l,l+1}] = \eta_T \tau(\mathbf{u}) \mathbf{v}_{l,l+1} \cdot \boldsymbol{\chi}_{l,l+1}, \quad (6)$$

$$[\mathbf{u}_f \cdot \mathbf{v}_{l,l+1}] = \alpha \eta_N \left( -\tau(\mathbf{u}) \mathbf{v}_{l,l+1} \cdot \mathbf{v}_{l,l+1} + \frac{1}{\tilde{B}} \frac{1}{2} \left( (-p_f^{(l+1)}) + (-p_f^{(l)}) \right) \right) \Pi, \quad (7)$$

$$(-p_f^{(l+1)}) - (-p_f^{(l)}) = \frac{i\omega\mu\Pi}{\hat{\kappa}} \frac{1}{2} \left( \mathbf{u}_f^{(l+1)} + \mathbf{u}_f^{(l)} \right) \cdot \mathbf{v}_{l,l+1} \quad (8)$$

$$\tau(\mathbf{u}) \mathbf{v}_{l,l+1} \cdot \mathbf{v}_{l,l+1} = \tau(\mathbf{u}) \mathbf{v}_{l+1,l} \cdot \mathbf{v}_{l+1,l} \quad (9)$$

$$\tau(\mathbf{u}) \mathbf{v}_{l,l+1} \cdot \boldsymbol{\chi}_{l,l+1} = \tau(\mathbf{u}) \mathbf{v}_{l+1,l} \cdot \boldsymbol{\chi}_{l+1,l}. \quad (10)$$

Here  $\eta_N$  and  $\eta_T$  are the normal and tangential fracture compliances, respectively and  $\hat{\kappa} = \kappa/h_f$ . The fracture dry plane wave modulus  $H_m = K_m + (4/3)G$  and the dry fracture shear modulus  $G$  are defined in terms of the fracture aperture  $h_f$  and the fracture compliances as  $\eta_N = \frac{h_f}{H_m}$ ,  $\eta_T = \frac{h_f}{G}$ . Besides,  $\Pi(\varepsilon) = \tanh \varepsilon/\varepsilon$ ,  $\tilde{B} = (\alpha M)/H_U$  ( $H_U$  is the undrained plane wave modulus) and

$$\varepsilon = \frac{(1+i)}{2} \left( \frac{\omega\mu\alpha\eta_N}{2\tilde{B}\hat{\kappa}} \right)^{1/2}, \quad \alpha = 1 - K_m/K_s.$$

A horizontally fractured Biot medium behaves as a TIV medium with vertical symmetry axis at long wavelengths. The stress-strain relations of the equivalent TIV medium are Carcione (2007)

$$\sigma_{11}(\tilde{\mathbf{u}}_s) = p_{11} \varepsilon_{11}(\tilde{\mathbf{u}}_s) + p_{12} \varepsilon_{22}(\tilde{\mathbf{u}}_s) + p_{13} \varepsilon_{33}(\tilde{\mathbf{u}}_s), \quad (11)$$

$$\sigma_{22}(\tilde{\mathbf{u}}_s) = p_{12} \varepsilon_{11}(\tilde{\mathbf{u}}_s) + p_{11} \varepsilon_{22}(\tilde{\mathbf{u}}_s) + p_{13} \varepsilon_{33}(\tilde{\mathbf{u}}_s), \quad (12)$$

$$\sigma_{33}(\tilde{\mathbf{u}}_s) = p_{13} \varepsilon_{11}(\tilde{\mathbf{u}}_s) + p_{13} \varepsilon_{22}(\tilde{\mathbf{u}}_s) + p_{33} \varepsilon_{33}(\tilde{\mathbf{u}}_s), \quad (13)$$

$$\sigma_{23}(\tilde{\mathbf{u}}_s) = 2 p_{55} \varepsilon_{23}(\tilde{\mathbf{u}}_s), \quad (14)$$

$$\sigma_{13}(\tilde{\mathbf{u}}_s) = 2 p_{55} \varepsilon_{13}(\tilde{\mathbf{u}}_s), \quad (15)$$

$$\sigma_{12}(\tilde{\mathbf{u}}_s) = 2 p_{66} \varepsilon_{12}(\tilde{\mathbf{u}}_s). \quad (16)$$

Here  $\tilde{\mathbf{u}}_s$ ,  $\boldsymbol{\sigma}(\tilde{\mathbf{u}}_s)$  and  $\boldsymbol{\varepsilon}(\tilde{\mathbf{u}}_s)$  are the displacement, the stress and the strain tensor at the macroscale, respectively.

To determine the complex and frequency dependent stiffness coefficients  $p_{IJ}(\omega)$  in (11)-(16), we applied five HFE compressibility and shear tests on 2D representative samples of fractured poroelastic materials. Each test consists on solving Biot's equations (3) with the fracture B. C. (5)-(10) and additional B. C. representing the HFE compressibility and shear tests. A detailed description of the HFE tests can be found in (Carcione, J. M. et al., 2011) and (Santos, J. E. et al., 2011).

### NUMERICAL EXAMPLES

In the first experiment we validate the results obtained modeling the fractures using the B. C. (5)-(10) with those obtained modeling the fractures as very thin layers. We used a square

Rock properties			
	Material 1	Material 2	Material 3
$K_s$ (GPa)	36	36	36
$\rho_s$ (Kg/m <sup>3</sup> )	2700	2700	2700
$\phi$	0.15	0.5	0.65
$K_m$ (GPa)	9.0	0.0055	0.0044
$\mu$ (GPa)	7.0	0.0033	0.0022
$\kappa$ (D)	0.1	10.0	20.0

Table 1: Physical properties of the solid materials used in the numerical examples

sample of side length 2 m, with 9 equally spaced fractures of aperture  $h_f = 1$  mm. The sample was discretized with a  $100 \times 109$  nonuniform mesh when modeling fractures as thin layers and a  $100 \times 100$  uniform mesh when fractures were represented using (5)-(10). The sample contains Material 1 in the background and Material 2 in the fractures, taken from Nakawa, S. and Schoenberg, M. A. (2007). In this example, we consider a brine saturated sample, with brine having density  $\rho_f = 1040$  kg/m<sup>3</sup>, viscosity  $\mu = 0.0018$  Pa·s and bulk modulus  $K_f = 2.25$  GPa.

Figures 1 and 2 show polar plots of the quality factors and energy velocity vectors for qP, qSV and SH waves as functions of the propagation angle at 60 Hz. Here 0 degrees and 90 degrees correspond to waves arriving parallel and normal to the fracture layering, respectively. A very good agreement between the numerical and analytical curves is obtained for all angles. The qP curves show strong attenuation for waves arriving normal to the fracture layering. The qSV wave has no loss along the directions parallel and normal to the fracture layering, showing maximum attenuation at about 45 degrees. In Figure 2 is seen that qSV and SH waves have stronger velocity anisotropy than qP waves, with qSV waves having the typical cuspidal triangles (or triplications), observed previously in fractured media (Carcione, 1996).

The second experiment considers the same sample and mesh size of the first experiment, with fractures are modeled using the B. C. (5)-(10) but for two different fractures apertures,  $h_f = 5$  mm and  $h_f = 0.5$  mm. The saturating fluid in the background is gas with density  $\rho_f = 500$  kg/m<sup>3</sup>, viscosity  $\mu = 2.0 \cdot 10^{-5}$  Pa·s and bulk modulus  $K_f = 0.025$  GPa. The fractures are saturated with brine.

Figures 3, 4 and 5 show energy velocities for qP, qSV and SH waves, respectively. Frequency is 60 Hz. It is observed an increase in anisotropy as fracture aperture increases. Also, energy velocities of all waves decrease at angles close to 90 degrees, i.e., for waves arriving normally to the fracture layering.

Finally, the third experiment performs a sensitivity analysis

## Anisotropy induced by fractures in porous media

using the B. C. (5)-(10) to study velocity variations in fractured poroelastic samples due to changes in volume fractions of Material 3 in the samples, a highly permeable and compliant material that is fractally distributed both in background and fractures.

The fractal samples are squares with side length 2 m and 9 equally spaced fractures of aperture  $h_f = 1$  mm. Both background and fractures are brine-saturated and a  $100 \times 100$  uniform mesh was used. Figure 6 displays the porosity spatial distribution in the background of the fractal sample for the case of 10% volume fraction of Material 3. Note that fracture properties also vary in fractal form.

Figures 7, 8 and 9 show that energy velocities in the fractal samples decrease as the volume fraction of Material 3 increases, an expected results because of the properties of this Material. Besides, qP and qSV waves tend to behave isotropically as the volume fraction of Material 3 increases, while SH energy velocity remains anisotropic.

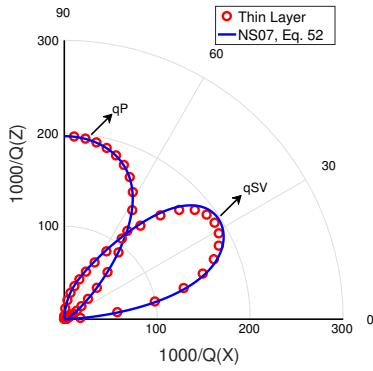


Figure 1: Dissipation factor of qP and qSV waves at 60 Hz. Fracture aperture is  $h_f = 1$  mm. The saturant fluid is brine in background and fractures. The solid line indicate the numerical values.

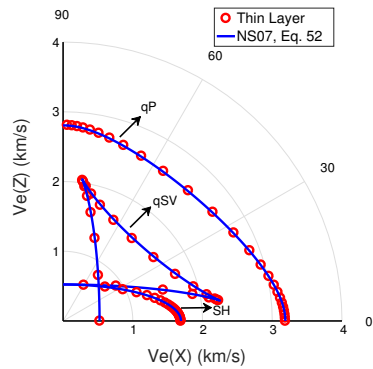


Figure 2: Polar representation of the energy velocity vector at 60 Hz for qP, qSV and SH waves. Fracture aperture is  $h_f = 1$  mm. The saturant fluid is brine in background and fractures. The solid line indicate the numerical values.

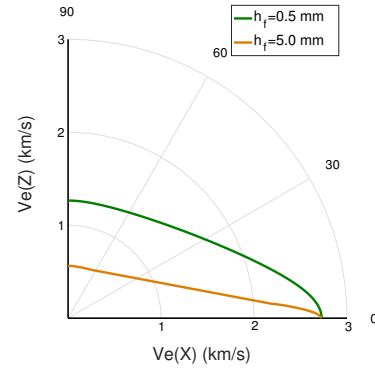


Figure 3: Polar representation of the qP energy velocity vector at 60 Hz. The saturant fluid is gas in background and brine in fractures. The solid line indicate the numerical values.

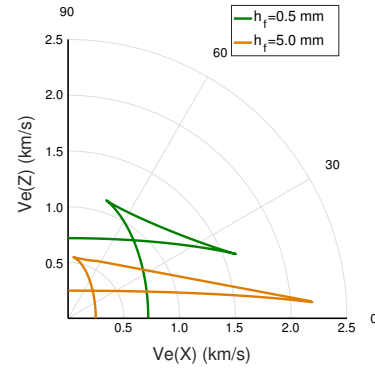


Figure 4: Polar representation of the qSV energy velocity vector at 60 Hz. The saturant fluid is gas in background and brine in fractures.

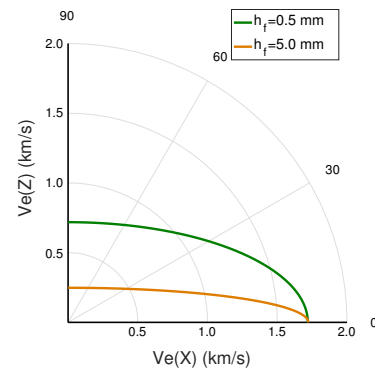


Figure 5: Polar representation of the SH energy velocity vector at 60 Hz. The saturant fluid is gas in background and brine in fractures.

## Anisotropy induced by fractures in porous media

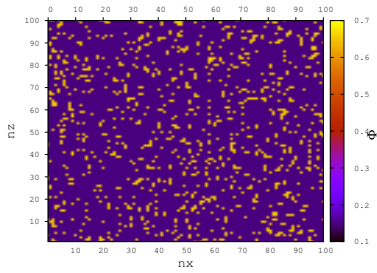


Figure 6: Porosity spatial distribution in the background of the fractal sample for the case of 10% volume fraction of Material 3.

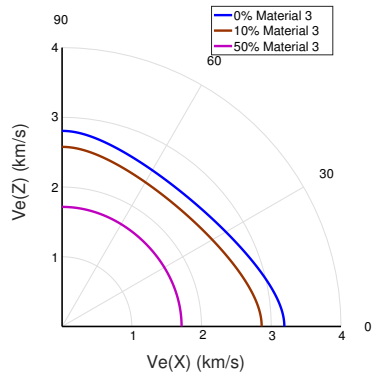


Figure 7: Polar representation of the qP energy velocity vector at 60 Hz for the case of a fractal sample. Background and fractures are saturated with brine. Fracture aperture is  $h_f = 1$  mm.

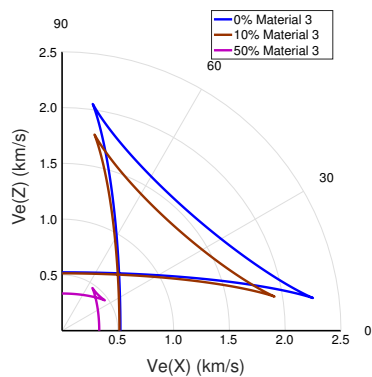


Figure 8: Polar representation of the qSV energy velocity vector at 60 Hz for the case of a fractal sample. The background and fractures are saturated with brine. Fracture aperture is  $h_f = 1$  mm.

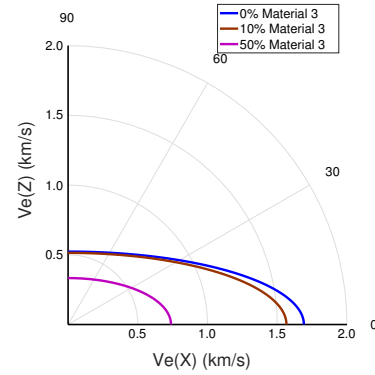


Figure 9: Polar representation of the SH energy velocity vector at 60 Hz for the case of a fractal sample. The background and fractures are saturated with brine. Fracture aperture is  $h_f = 1$  mm.

## CONCLUSIONS

This work used a Finite Element procedure to determine the five complex and frequency-dependent stiffnesses of a transversely isotropic and viscoelastic medium long-wave equivalent to a highly heterogeneous horizontally fractured Biot medium, with fractures represented as boundary conditions. It is worth to emphasize that is computationally very convenient to use B. C. to model fractures, because if fractures were to be represented instead as fine layers, much smaller meshes would be needed to discretize the fine layers than those required to discretize the background. The procedure was first validated comparing the results with those obtained for fractures modeled as fine layers. Then it was applied to analyze the sensitivity of velocities to variations in fracture aperture and proportions of fractal heterogeneities present in the fractured poroelastic samples. In all cases, the experiments show that fractures induce strong velocity anisotropy. Large increase in anisotropy was observed for large increases in the openings of the fractures. Also, energy velocities for qP and qSV waves were observed to decrease as the volume fraction of the fractal heterogeneities increase, with these two waves tending to behave isotropically. Besides, SH energy velocities remained anisotropic even for large volume fractions of fractal heterogeneities. The results of the last two experiments suggest that this FE procedure may become an useful tool to study variations of velocities in hydrocarbon reservoirs subject to hydraulic fracturing.

## Anisotropy induced by fractures in porous media

### REFERENCES

- Biot, M.A., 1962, Mechanics of deformation and acoustic propagation in porous media: *Journal of Applied Physics*, **33**, 1482–1498.
- Carcione, J. M., 1996, Plane-layered models for the analysis of wave propagation in reservoir environments I: *Geophysical Prospecting*, **44**, 3–26.
- , 2007, Wave fields in real media: Wave Propagation in Anisotropic, Anelastic, Porous and Electromagnetic Media, *Handbook of Geophysical Exploration*, vol. 38: Elsevier (2nd edition, revised and extended).
- Carcione, J. M., Santos, J. E., and Picotti, S., 2011, Anisotropic poroelasticity and wave-induced fluid flow. Harmonic finite-element simulations: *Geophysics Journal International*, **186**, 1245–1254.
- Gelinsky, S. and Shapiro, S. A., 1997, Poroelastic Backus-averaging for anisotropic, layered fluid and gas saturated sediments: *Geophysics*, **62**, 1867–1878.
- Gurevich, B., 2003, Elastic properties of saturated porous rocks with aligned fractures: *Journal of Applied Geophysics*, **54**, 203–218.
- Gurevich, B., Brajanovski, M., Galvin, R. J., Müller, T. M., and Toms-Stewart, J., 2009, P-wave dispersion and attenuation in fractured and porous reservoirs—poroelasticity approach: *Geophysical Prospecting*, **57**, 225–237.
- Krzkikalla, F. and Müller, T., 2011, Anisotropic P-SV-wave dispersion and attenuation due to interlayer flow in thinly layered porous rocks: *Geophysics*, **76**, WA135.
- Nakawa, S. and Schoenberg, M. A., 2007, Poroelastic modeling of seismic boundary conditions across a fracture: *Journal of the Acoustical Society of America*, **122**, 831–847.
- Santos, J. E., R. M. Corredor, and J. M. Carcione, 2014, Seismic velocity and q anisotropy in fractured poroelastic media: *International Journal of Rock Mechanics and Mining Sciences*, **70**, 212 – 218.
- Santos, J. E., Carcione, J. M., and Picotti, S., 2011, Analysis of mesoscopic loss effects in anisotropic poroelastic media using harmonic finite element simulations: 81th Annual International Meeting, SEG, Expanded Abstracts, 2211–2215.